$H^0(n=3,4)$ Stark states produced in the interaction of 800-MeV H^- ions with thin foils

P. B. Keating,* M. S. Gulley, H. C. Bryant, E. P. MacKerrow, W. A. Miller, and D. C. Rislove
University of New Mexico, Albuquerque, New Mexico 87131-1156

Stanley Cohen, J. B. Donahue, D. H. Fitzgerald, David J. Funk, S. C. Frankle, R. L. Hutson, R. J. Macek, M. A. Plum, N. G. Stanciu, O. B. van Dyck, and C. A. Wilkinson
Los Alamos National Laboratory, Los Alamos, New Mexico 87545

(Received 4 April 1997; revised manuscript received 16 July 1998)

The interaction of 800-MeV H^- ions with a thin foil produces protons, the ground state and excited states of neutral H^0 atoms, and unstripped H^- ions. We investigated the distributions of individual H^0 Stark states within the $n=3$ and 4 levels produced by C and Al_2O_3 foil stripping of H^- ions. Foils of various thicknesses were placed upstream of a magnet with a linearly increasing transverse field along the beam direction producing a motional electric field strong enough to ionize H^0 states with $n \geqslant 3$. We consider three questions: (i) What are the populations of individual H^0 Stark states produced in the interaction of 800-MeV H^- ions with thin C and Al_2O_3 foils, (ii) how do the relative population distributions change with foil thickness, and (iii) how is the population distribution produced in an Al_2O_3 foil modified when the foil is placed in a magnetic field? A simple qualitative model is presented to explain the major trends. [S1050-2947(98)02212-4]

PACS number(s): 34.50.Fa, 33.55.Be, 41.20.−q, 41.75.Cn

I. INTRODUCTION

The passage of an ion beam through a thin foil is an interesting example of an ion-solid interaction having both theoretical and practical implications. A classical transport theory employing a Monte Carlo solution to a microscopic Langevin equation to describe the multiple scattering inside the foil [1] was extended to the relativistic regime by Gervais *et al.* [2]. This theory was compared with recent experimental data of Gulley *et al.* [3], of which the present work is an extension, and agreement was found. The theory was developed to predict the single- and double-electron detachment from the H^- ion and also the evolution of excited H^0 states, described by the principal quantum number n, as a function of foil thickness. Recently, Kürpick *et al.* extended the theoretical investigations in [2] to include the production of individual H^0 Stark states produced in the interactions of high-energy H^- ions with thin foils [4].

An important application for this work is in accelerator physics where foils are commonly used to strip an electron from H^- to produce H^0, which may be further stripped to a bare proton for injection into a proton storage ring. Some H^0 Stark states, created in the foil, field ionize in the motional electric field produced by downstream bending magnets. The protons derived from these field-ionized states pose problems for injection into proton storage rings, such as the Los Alamos Meson Physics Facility (LAMPF) Proton Storage Ring (PSR), since their trajectories may be outside the acceptance of the ring, causing first-turn losses and activation of beam line components [5,6]. Furthermore, the radiation levels produced by the errant particles colliding with the walls can seriously limit currents. The relative abundances of individual Stark states produced in the interaction of relativistic H^- ions with thin foils have never been measured. Within a given n level there are significant differences in lifetimes against field ionization in the rest frame electric field. To calculate accurately the first-turn injection losses into the PSR, the relative abundances of the individual Stark states within the relevant n levels must be determined.

We use field stripping, a source of difficulty for injection into storage rings, as a tool for measuring Stark state populations in motional electric fields. In this work there are three principal questions we wish to answer. First, what are the populations of individual H^0 Stark states produced in the interaction of 800-MeV H^- ions with thin C and Al_2O_3 foils? Second, do the relative population distributions change with foil thickness? Finally, does the population distribution change when a magnetic field is imposed on an Al_2O_3 foil?

Most of the work in atom beam-foil interactions has been done at beam energies lower than the 800 MeV used in this measurement. Electronic excited-state populations produced in beam-foil interactions exhibit a nonexponential decay law [7] imposed by cascades from highly excited atoms. Subsequent calculations account for the effects of the cascades and predict that fast ions emerging from the solid appear in high-l Rydberg states [8,9]. Unlike the ion-solid interaction, binary ion-atom collisions at similar high velocities populate mainly low-l states [10]. A classical transport theory by Kemmler, Burgdörfer, and Reinhold to explain the passage of O^{2+} (2-MeV/nucleon) through carbon foils [10] has been successfully applied to the experimental data of Yamazaki *et al.* [11], where (1.5–5)-MeV carbon ions traversed carbon foils and He gas. The high-l distribution in the $n=5$ shell of carbon was satisfactorily explained by the theory of Kemmler, Burgdörfer, and Reinhold. This theory predicts that the high-l states are preferentially produced in ion-solid collisions due to the stochastic scattering of the highly excited electrons in the solid [10].

This work is a continuation of an earlier study [12,13] to

*Permanent address: Physical Sciences Incorporated, 20 New England Business Center, Andover, MA 01810.

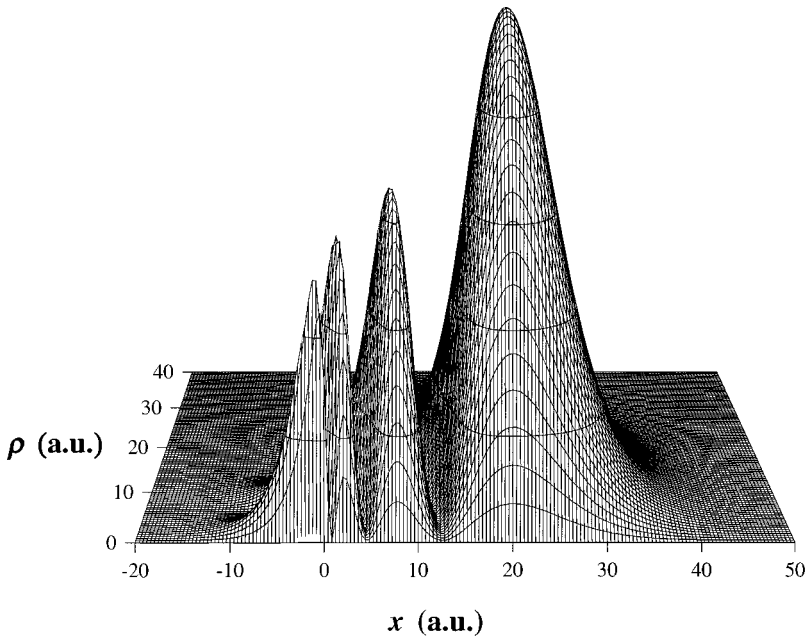

FIG. 1. Normalized charge density of the parabolic state $|n=4, n_1=3, n_2=0, m=0\rangle$. The field points are along the x axis. The charge plotted is $2\pi\rho$ times the charge per unit volume. The dipole moment is 18 a.u.

determine the nature of the interaction of relativistic H^- beams with thin foils. Preliminary results of this work, done at the High Resolution Atomic Beam Facility (HIRAB) at the LAMPF, have been presented elsewhere [14]. The populations within a given n level for carbon foil thicknesses ranging from 9 to 553 $\mu g/cm^2$ were reported by Gulley *et al.* [3], along with a theory by Gervais *et al.* [2], which was shown to be in agreement with the experimental results. The results reported here concern the population fractions of the individual Stark states within the $n=3$ and 4 levels.

II. THEORY

The interactions of a relativistic H^- ion beam traversing a thin foil include inelastic and elastic scattering, single- and double-electron detachment from H^-, and the production and evolution of excited H^0 states in the foil. The model that predicts populations distributions within a given n level [2] treats the H^- ion-foil interaction as a series of incoherent collisions and at present cannot predict Stark state distributions and thus may not be entirely appropriate. The time between collisions of an 800-MeV H^0 atom with 2.2-Å-spaced foil atoms is 4.7×10^{-19} s in the ion rest frame, about 300 times shorter than the atomic unit of time 1.37×10^{-16} s. Since the period τ_n of an electron in a Bohr orbit scales as n^3 [16], an electron in a $H^0(n=3,4)$ atom traversing a foil could be bombarded many times in a single orbital period.

Field ionization is used to determine the populations of H^0 Stark states produced in the foil. A uniform electric field partially removes the degeneracy of hydrogenic states, with the degeneracy in m remaining. Arbitrarily weak fields transform stationary states into narrow quasistationary bands in the continuum into which an electron may tunnel. Each energy level is characterized by its width $\Gamma=\hbar/\tau$, which increases with the field intensity and is inversely proportional to its lifetime τ. The Schrödinger equation for an electron subject to a Coulomb potential $-Ze^2/r$ may be uncoupled into two ordinary differential equations using parabolic coordinates (ξ,η,ϕ) defined in [15]. This uncoupling also holds when a homogeneous external electric field F in the z direction is present. The solutions of the Schrödinger equation may be described in terms of the parabolic quantum numbers n, n_1, n_2, and m, which are related by

$$n=n_1+n_2+|m|+1, \tag{1}$$

where n is the principal quantum number, m is the magnetic quantum number, and n_1 and n_2 are non-negative. The so-called electric quantum number $k\equiv n_1-n_2$ is also commonly used and will be mentioned below. The parabolic state wave

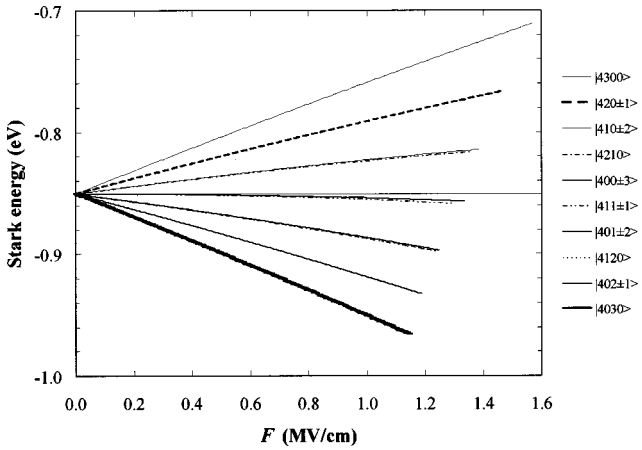

FIG. 2. Stark energies of H^0 Stark states in the $n=4$ level versus the rest frame electric field based on the ''modified'' Damburg-Kolosov fifth-order perturbation theory. The maximum field shown for each state is the approximate field value by which the state has decayed due to field ionization to only 0.1% of its original population.

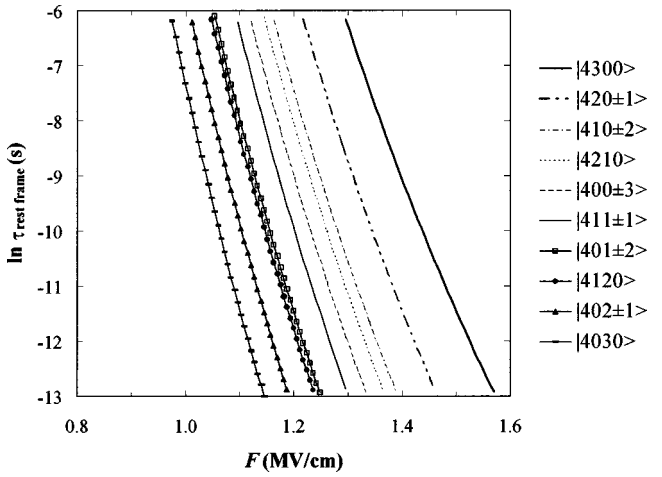

FIG. 3. Rest-frame lifetimes against field ionization of H^0 Stark states in the $n=4$ level versus the rest frame electric field based on the modified Damburg-Kolosov fifth-order perturbation theory. The lifetimes shown are in the range 10^{-6}–10^{-13} s.

functions are azimuthally symmetric about the field direction. The charge densities of the parabolic coordinate wave functions, unlike their spherical state counterparts, have permanent electric dipole moments d along the field direction z. States with high $|k|$ have the highest magnitude of d. When k is positive (negative) the dipole moment is along the positive (negative) field direction. Figure 1 shows the normalized (unit volume under the surface) charge density of state $|n=4, n_1=3, n_2=0, m=0\rangle$ as an example. The charge density is the absolute magnitude of the squared wave function times $2\pi\rho$, where ρ is the perpendicular distance from the quantization axis. The moment of the charge density along the field direction is 18 a.u.

The lifetimes of individual H^0 Stark states against field ionization as a function of electric field were calculated based on the work of Damburg and Kolosov [16], whose perturbation theory extends to fifth order in the field F. We describe later how these predictions were modified. The Stark energies and lifetimes against field ionization as a function of electric field for the $n=4$ level based on a modified Damburg-Kolosov perturbation theory (DKPT) are shown in Figs. 2 and 3, respectively. The energy splitting in eV between the states with the extreme values of k within a level n is approximately

$$\Delta E_n \approx 3F \frac{n(n-1)}{Z} (5.29\times 10^{-3}) \text{ eV}, \tag{2}$$

where the field F is expressed in MV/cm.

In this experiment a static laboratory magnetic field gave rise to a rest frame motional electric field plus a rest frame magnetic field. Qualitatively, a magnetic field tends to increase the binding of the electron by forcing the electron

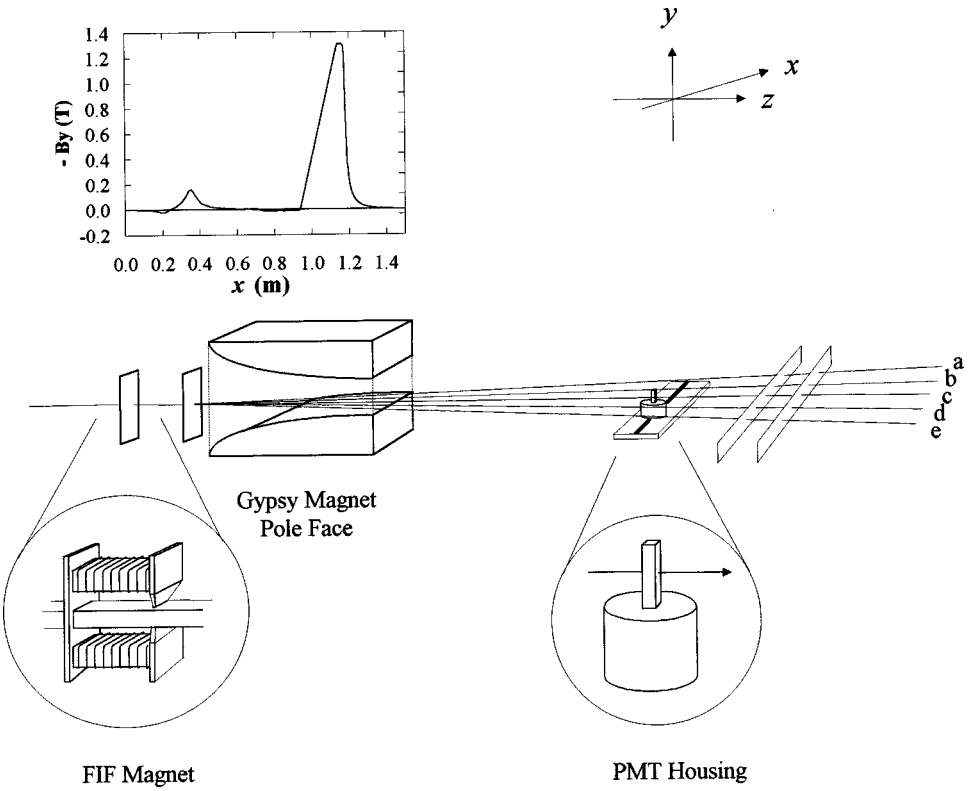

FIG. 4. Diagram showing the possible outcomes of interactions of H^-, H^0, and H^+ with the foil and ''Gypsy'' magnet. The various charge states are separated and detected 5.5 m from the peak magnetic field with a scanning scintillator in coincidence with two wide scintillators. The scanning scintillator travels along the x direction, both magnetic fields point in the negative y direction, and the incident beam defines the z direction. An aluminum window at the end of the drift tube (not shown) strips all electrons from H^0 and H^- so that only protons are detected. Protons that enter the Gypsy magnet are detected at position a and protons derived from field-detached H^- and H^0 states not field stripped, field-stripped H^0 states, and H^- not field detached appear at positions b, c, d, and e, respectively. PMT denotes photomultiplier tube.

closer to the nucleus. The direct effect of magnetic fields on H^- in its singlet ground state is restricted to the nuclear magnetic moment; the effect on atomic hydrogen is 10^3 larger, but nevertheless is still negligible. We are unaware of a quantitative theory describing the effects of a relatively weak magnetic field (<1 a.u.) on the electric-field ionization of H^0.

III. EXPERIMENTAL METHOD

The basic idea as shown in Fig. 4 was to send an 800-MeV H^- beam onto a foil and to examine the results. The excited states of neutral H^0 produced in the foil are stripped in the motional linear-gradient field of a downstream magnet (named ''Gypsy'') and the resulting distribution of ''daughter'' protons is dispersed transverse to the incident beam direction. The field of the Gypsy magnet, which was used in previous studies [3,17], was oriented perpendicularly to the incident H^- and increased linearly in strength along the beam direction. H^0 states stripped at various field strengths according to their lifetimes against field ionization and the resultant electrons and protons were deflected in the field. The protons were detected with a scanning scintillator in coincidence with a pair of paddle-shaped scintillators that covered the entire exit window and whose signals were used for normalization. From the lifetime calculations and the known magnetic-field map (Fig. 4), the trajectories of the protons derived from the stripped H^0 states were calculated and compared with the experimental data. These experiments were performed under two conditions. Most of our work concerned interactions of H^- with a foil in a field-free region just upstream of the Gypsy magnet. The second set of experimental conditions were those of the foil-in-the-field (FIF) experiments. In the FIF experiments, the foil, instead of residing just upstream of the Gypsy magnet, was placed in the housing of an additional magnet (FIF magnet) 0.6 m upstream of the Gypsy foil box. The drift distance allowed the H^0 Stark states produced in the FIF foil to evolve, redistributing their populations within the various m sublevels before encountering the Gypsy field.

Strong ion rest frame electric fields were produced with the FIF and Gypsy electromagnets. A laboratory magnetic field $\mathbf{B}_{\rm lab}$ transforms as a rest frame electric field $\mathbf{F}_{\rm rest}$, plus a rest frame magnetic field $\mathbf{B}_{\rm rest}$ [18]. The rest frame electric field is given by $\mathbf{F}_{\rm rest}=\gamma\mathbf{v}\times\mathbf{B}_{\rm lab}$, where $\mathbf{v}$ is the ion's velocity in the laboratory frame and the rest frame magnetic field is given by $\mathbf{B}_{\rm rest}=\gamma\mathbf{B}_{\rm lab}$. The parameter $\gamma=T/Mc^2+1$, where T is the energy of the beam and Mc^2 is the rest energy of the H^- ion. For a beam energy of 797 MeV ($\gamma=1.85$), a 1-T laboratory magnetic field results in a rest frame electric field of 4.67 MV/cm. The typical momentum spread of the LAMPF H^- beam was estimated to be $\delta p/p\sim10^{-4}$ based on previous experiments [12]. The beam energy was not measured directly for these experiments, but a nominal value of 797 ± 2 MeV was typical for the HIRAB laboratory at LAMPF. The macropulse rate was 118 Hz and the macropulse length was 725 μs, with a hybrid structure consisting of seven repeated patterns of 35 ns of 5-ns spaced micropulses, followed by 65 ns without micropulses.

The field map and a sketch of the FIF magnet are shown in Fig. 4. The full width at half maximum (FWHM) of the

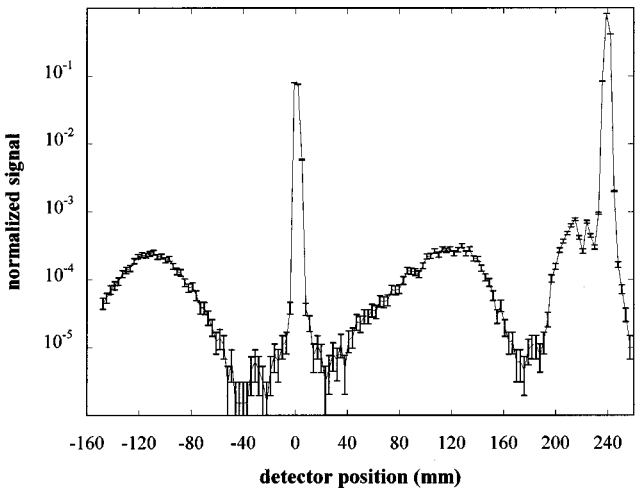

FIG. 5. Normalized signal $(H2\cdot S1\cdot S2)/(S1\cdot S2)$ vs detector position x plotted on a logarithmic scale. The error bars indicate the standard deviations for each data point. The Gypsy magnet was set to a peak field of 1.3 T to separate the $n=3$ level from those of higher n. The FIF magnet was set to 0.16 T. The broad feature peaked near -100 mm is due to field-detached H^-, the narrow peak at $x=0$ is due to unstripped H^0, and the broad feature peaked near 120 mm is due to field-stripped $n=3$ states. The peak due to protons is centered near 240 mm and the shoulder appearing on the lower-x-value side of the H^+ peak is due to field ionization of H^0 states in levels $n>3$.

FIF field is about 4 cm along the beam direction. The magnet housing was placed around a rectangular (5×10 cm^2) beam pipe upstream of the Gypsy magnet. The Gypsy magnet is a half-quadrupole magnet turned 90° from the usual orientation of a quadrupole, producing a field that increases linearly with distance along the beam direction. The fields of the two magnets were parallel and directed downward (taken to be the y direction). The peak field was remotely set to a field value optimized to strip a particular n level: 1.3 T to separate the $n=3$ states from the higher-n states and 0.6 T to separate the $n=4$ states from the other higher-n states. The peak field was monitored with a shunt resistor whose output voltage was used in the calibration of the magnet. No appreciable stripping of $n=2$ or 1 states occurred. About 30% of state $|3200\rangle$ remained unstripped through the 1.3-T Gypsy field; all other states in the $n=3$ level were completely stripped, as were all states in the $n=4$ level in the 0.6-T field. All states in the $n=5$ level were completely stripped in a 0.29-T field, but the individual Stark states could not be resolved in our experiments.

The foils (dimensions 2.5×7.5 cm^2) were glued to thin 2.5×7.5 cm^2 aluminum plates having 2-cm-diam circular holes through their centers. There were two foil boxes: one near the Gypsy magnet (the Gypsy foil box) and another for the FIF experiment 0.6 m further upstream. The Gypsy foil box had two remotely actuated U-shaped foil carriers, called forks, each of which held five foils. The forks were placed about 5 cm apart along the beam direction. The foils were remotely positioned in the beam path. The double-fork configuration also allowed ''double-foil'' experiments to be performed. A foil on each fork could be positioned in the beam path so that the H^- beam could impinge on two foils. The FIF foil box held a single Al_2O_3 foil with the fork oriented

horizontally. The position of the FIF foil, determined by the experimental deflection of the H^-, H^0, and H^+ beams, was near the peak field. The Al_2O_3 foils were made at the Appleton Rutherford Laboratory [19] and the carbon foils were produced commercially. The foil areal densities ($\mu g/cm^2$) were measured using α ranging [20]. Although both carbon and Al_2O_3 foils were used in the Gypsy foil box, only one foil, an Al_2O_3 foil of areal density 167 $\mu g/cm^2$, was tested in the FIF foil box. All foils survived the experiments intact.

A 5-m-long, stainless-steel, rectangular cross-section drift tube was located downstream of the Gypsy magnet. A 0.13-mm-thick aluminum exit window stripped all electrons from the incident H^-, H^0, and H^+ beams as they emerged from the drift tube, producing protons that were detected by the scintillator detectors, as described below. For a peak Gypsy field of 1.3 T, the angle between the undeflected $H^0(n=1,2)$ peak (maximum) and the peak from protons that entered the Gypsy magnet was approximately 40 mrad.

Scintillators downstream of the exit window were used to detect the protons that emerged from the exit window. Scintillators were chosen for their linear response for high counting rates and fast readout time when coupled with standard computer automated measurement and control (CAMAC) electronics. Two wide scintillators ($S1$ and $S2$) in fixed positions and in temporal coincidence with a 5.8-mm-wide scanning scintillator ($H2$) were used obtain the representative spectrum shown in Fig. 5. The scintillator $H2$ was approximately 5.7 m downstream of the beginning of the upstream ramp of the Gypsy field. The scintillators $S1$ and $S2$ counted all particles emerging from the exit window and were used for normalization. The abscissa of the normalized spectrum of Fig. 5, denoted by $(H2 \cdot S1 \cdot S2)/(S1 \cdot S2)$, is the coincidence rate between the scanning scintillator $H2$ with the paddle scintillators $S1$ and $S2$, divided by the coincidence rate between $S1$ and $S2$. The coincidence between $H2$, $S1$, and $S2$ discriminated against unwanted background signals. The scanning scintillator $H2$ was mounted on a translation stage coupled to a drive screw. A stepper motor controlled by a personal computer turned the drive screw to position scintillator $H2$. Each data point was taken at fixed $H2$ position until the $S1$ signal reached a set maximum number of counts (about 6.5×10^5). With the beam parameters used, the probability of counting two events as a single event was below 10^{-4}. The scanning scintillator was moved along the x direction in equal steps (either 2 or 3 mm for an entire spectrum) covering the H^- peak through the proton peak. The personal computer also controlled the data acquisition via interface with CAMAC modules. The HIRAB laboratory beam-line pressure was approximately 10^{-7} torr.

IV. DATA ANALYSIS

A. Calculations of the dP/dx for the H^0 Stark states

The stripping probabilities of the H^0 Stark states in a given n level as a function of field and their probability density distribution function (PDDF) curves along the travel direction of the scanning scintillator were computed. Since decay of an individual Stark state occurs by field ionization and by spontaneous emission, both loss mechanisms are calculated and incorporated into the PDDF for each Stark state as described below.

The stripping probability calculation was based on a single-ion code. In order to compare the theoretical predictions with the experimental data, the finite beam width (~1 mm FWHM) and the detector response function were convolved with the theoretical predictions. The detector response function and the ion beam width were determined using a multiparameter modified Levenberg-Marquardt fitting algorithm [21] to data obtained in runs taken with a small step size designed to determine the beam profile. The detector was modeled as having a straight-edged response with a Gaussian top and both the width of the straight edged part and the Gaussian width were varied. The ion beam intensity was assumed to be Gaussian. The two other variable parameters were an arbitrary normalization factor and a shift parameter that specified the peak of the convolution. The beam width and the detector response function parameters from the fitting procedure were used later for convolving with the theoretical probability distribution functions. The detector width determined from the fit was close to the measured width of the plastic scintillator material of the scanning scintillator and the beam width was also close to the width measured in previous experiments.

For a given n level, the data in the region between the protons derived from unstripped H^0 atoms and the protons at the maximum bend angle resulted from a superposition of $n(n+1)/2$ distinct states (reduced from n^2 states due to the degeneracy in m) that stripped in the Gypsy field. The DKPT did not take into account effects on the lifetime calculations due to magnetic fields (in our case $\gamma B_{\rm lab}$). For each state within a given n level, the population fraction P as a function of z and the corresponding PDDF were calculated. The PDDF curves for the $n=3$ and 4 levels shown in Fig. 6 were used in a fitting routine to calculate the populations of the respective states.

The experimental signal S_j at detector position x_j can be written

$$S_j = \sum_i a_i \frac{dP_i(x_j)}{dx}, \tag{3}$$

where x_j is the detector position, $dP_i(x_j)/dx$ is the value of the PDDF of Stark state i at detector position x_j, and $\{a_i\}$ is a set coefficients. The coefficients $\{a_i\}$ that minimized χ^2 were determined using a multiparameter fitting program written in the C language based on routines in Ref. [21].

Although calculating lifetimes of Stark states against field ionization using the DKPT is straightforward and produces reasonable estimates, improved accuracy has been achieved by several other approaches, including those of Damburg and Kolosov [16] and Bergeman [22]. These more complicated methods of calculating the lifetimes result in higher precision, but the complexity of the computer codes for calculations at the many field values necessary for smooth probability distribution functions nearly prohibits their use. We combined the computational ease of the DKPT with the results of the more accurate Bergeman calculations to make a modified perturbation theory [which shall hereafter be called the Bergeman-modified DKPT (BMDKPT)]. The idea was to relate the lifetimes from the DKPT (which were calculated at every field value of the interpolated magnetic field map con-

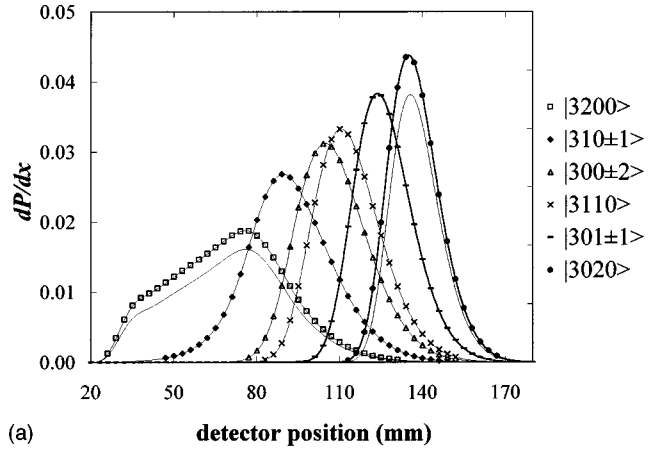

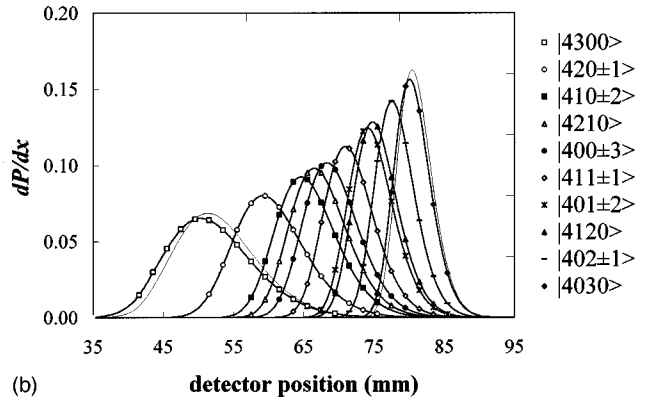

FIG. 6. Probability density distribution functions of the H^0 Stark states $|nn_1n_2m\rangle$ at a beam energy of 797 MeV in the (a) $n=3$ level through a 1.3-T peak Gypsy field and (b) the $n=4$ level through a 0.6-T peak Gypsy field. The states most resistant to field ionization appear at the lower values of the detector position x. The origin of the x axis is the undeflected H^0 peak. The markers indicate the scanning scintillator detector positions where experimental data were taken. The curves without markers are the distribution functions determined from the Damburg-Kolosov fifth-order perturbation theory without modification.

sisting of 13 000 points) with the results of Bergeman's calculations, which were calculated at a small number of points (fewer than ten for each state). For a given state, the widths were calculated using the DKPT at the same field values used in the Bergeman calculations. The ratio of the widths as function of field is given by

$$R(F)=1-NF\ \exp(CF^{1/2}), \tag{4}$$

where F is the field in a.u. and N and C are two parameters whose values were calculated by minimizing χ^2. This functional form was chosen since the two calculations should agree at the zero-field limit and the curvature of the ratio was well matched by the function in the region of field strengths where the states strip. The results do not depend strongly the choice of a functional form for $R(F)$. The population of a state as a function of field was calculated, as was its derivative with respect to field F, dP/dF. The fit parameters C and N for each state were calculated using the Bergeman results only in the field region where dP/dF was appreciable as determined by the unmodified DKPT. The widths of seven of

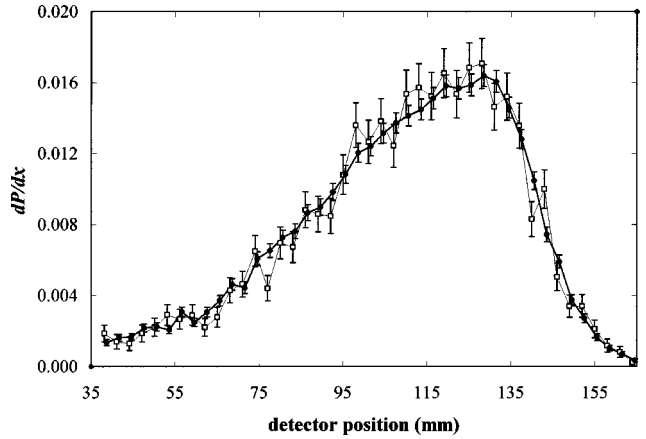

FIG. 7. Spectra comparing two carbon foils of thickness 9.4 and 107 μg/cm^2. Despite the order of magnitude difference in the foil thickness, apart from an overall normalization factor, the distributions have similar shapes.

the ten $n=4$ states were calculated by Bergeman. Estimates of $R(F)$ for the three remaining states were made by averaging the coefficients of the adjacent states (the order of the states was in terms of the peaks of their dP/dF versus F). The widths calculated by Bergeman were narrower than the DKPT widths, but within a factor of 2 in the field region of interest. The widths given by the ''exact'' calculation of Damburg and Kolosov were also narrower than their perturbation theory results. The Bergeman results are in close agreement with the exact results of Damburg and Kolosov.

Once the fit coefficients (C,N) of $R(F)$ were determined for each state, the widths as a function of field were calculated by multiplying the widths based on the DKPT, Γ_{DKPT}, by the ratio $R(F)$, giving the widths Γ_{BMDKPT}. The probability density distribution functions along the scanning scintillator direction dP/dx versus x were then computed using Γ_{BMDKPT}. Since the lifetimes calculated using the DKPT are shorter than those found by the BMDKPT for the same field strength, the net effect was that the dP/dx versus x curves shifted toward the unstripped H^0 peak and the shapes of the curves changed slightly, relative to the PDDF curves obtained using the unmodified DKPT. For the state most resistant to field ionization in the $n=4$ level, $|4300\rangle$, the peak of the dP/dx versus x curve moved about 1 mm closer to the unstripped H^0 peak. Smaller shifts were obtained for the other curves. A comparison of the dP/dx versus x curves using the DKPT and the BMDKPT widths for the states $|3200\rangle$ and $|3020\rangle$ and for the states $|4300\rangle$ and $|4030\rangle$ are shown in Figs. 6(a) and 6(b), respectively.

Two sets of fits were made for each of the levels $n=3$ and 4. The first set used six and ten PDDF curves for the $n=3$ and 4 levels, respectively. The second set of fits used the ''symmetry hypothesis,'' which posits that states within a given n level with equal $|k|$ are produced in equal abundance in the amorphous foil. The charge densities of these pairs of states are mirror images with respect to reflection in the xy plane. The PDDF curves of states with equal $|k|$ were fit with a single coefficient. For the $n=3$ level, there were two such pairs (for $|k|=2$ and 1) and for the $n=4$ level there were three pairs ($|k|=3,2,1$). Using the symmetry hypothesis,

there were four and six independent fit coefficients for the $n=3$ and 4 levels, respectively. Since the center of the convolution of the beam and detector was not known precisely, a shift in the origin of the PDDF curves was used as a free parameter. The χ^2 was determined as a function of the shift parameter taken in 0.5-mm increments.

B. Calculation of the spontaneous decay

Decays of excited H^0 states due to spontaneous emission were explicitly calculated. In the case of the FIF experiment, the distance between the foil and the beginning of the linear rise in the Gypsy field was 0.9 m (the distance between foil boxes was 0.6 m), allowing significant time for decay. The field-free matrix elements were calculated based on the formulas in Ref. [15]. The Stark energies as a function of field were calculated as described above and the transition rates from all upper states to all lower states were calculated. The spontaneous emission rate out of a particular state was added to the rate of decay due to field ionization.

Calculations showed that decays from higher-n levels into the $n=4$ level were negligible; only about 0.2% of the sparsely populated $n=5$ level decayed spontaneously in transit from the FIF magnet to the Gypsy magnet and only about 20% of that went to the $n=4$ level. The relative abundance of level n produced in a foil is expected to fall off as $1/n^3$ [12] and the transition probabilities decrease with increasing n, so that contributions from higher-n levels are even less important. Similar calculations showed that spontaneous decays to the $n=3$ level were also negligible. Slight differences in decays of states with opposite values of electric quantum number k arise because states with $-k$ are lost via field ionization sooner than their $+k$ counterparts, giving the latter states more time to decay via spontaneous emission. States in the $n=3$ level decayed between 5% and 13% when the foil was placed in the Gypsy foil box and between 10% and 27% when the foil was placed in the FIF foil box. States in the $n=4$ level decayed between 1.5% and 5% when the foil was placed in the Gypsy foil box, and between 3% and 11% when the foil was placed in the FIF foil box.

V. RESULTS AND ANALYSIS OF $H^0(n=3)$ STATES

A. Carbon foil raw data and analysis

The raw spectra for foils in the range 9.4–107.2 μg/cm^2 are shown in Fig. 7. These spectra have been renormalized so that their integrated areas [the integral of the normalized scintillator signal $(H2\cdot S1\cdot S2)/(S1\cdot S2)$ with respect to the position of scanning scintillator $H2$ along x] are equal to that of the raw spectrum of the 69.3-μg/cm^2 foil, whose integrated area was the largest of all the foils tested. Although the thicknesses differ by a factor of 11, apart from a normalization factor, the two spectra overlap. This tells us immediately that the distribution among Stark states is very similar. According to [3], the population fraction of $n=3$ states was $\sim$1% of the total beam for the 69.3-μg/cm^2 foil. Spectra from other foil thicknesses in this range were similar in shape to those shown in Fig. 7.

The relative abundance determined without using the symmetry hypothesis of the individual Stark states in the $n=3$ level produced at the foil are shown in Fig. 8(a). The

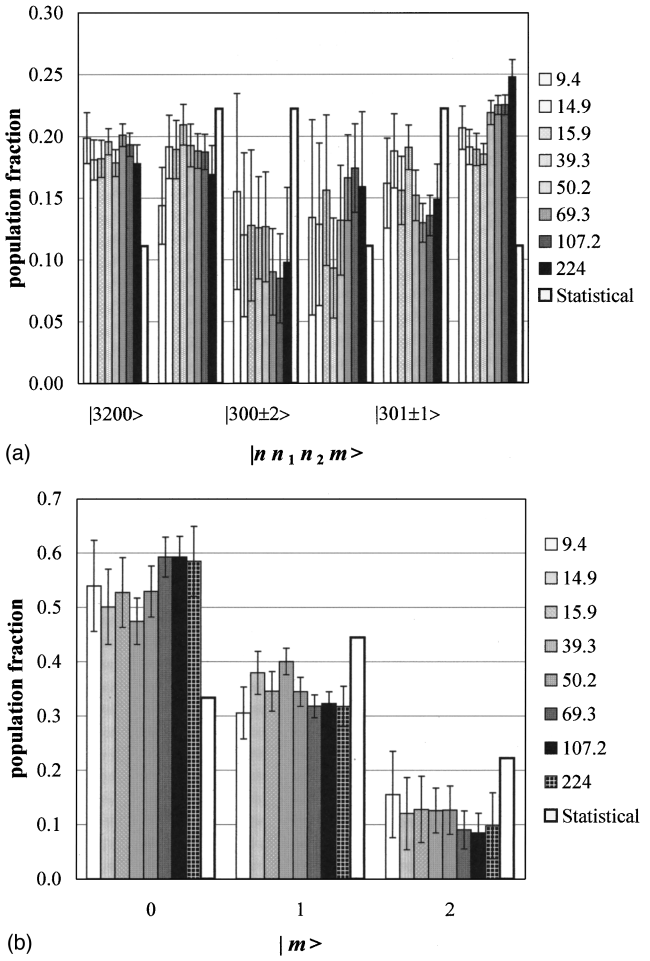

FIG. 8. (a) Population fractions at the foil of $H^0(n=3)$ states for various carbon foil thicknesses (shown in the legend in units of μg/cm^2). The values stated are the populations at the foil that include the depletion due to spontaneous decays between the foil and the Gypsy magnet. The fits are not constrained by the ''symmetry hypothesis'' in $|k|$. The statistical weights are also shown, where each state with $m\neq 0$ is weighted by $2/n^2$ and states with $m=0$ are weighted by $1/n^2$. (b) Populations in the m sublevel of the $n=3$ level based on the populations in (a). Populations for statistical weighting are also shown. A significantly higher population fraction resides in the $m=0$ sublevel compared to a statistical distribution.

populations in the m sublevels corresponding to the fits of Fig. 8(a) are shown in Fig. 8(b). The best-fit reduced χ^2 values were in the range 0.63–1.24 (average 0.942), indicating good fits. Thicker foils produced $n=3$ states less efficiently than the thinner foils above a thickness of 70 μg/cm^2 [3] and the fits for the foils of thickness greater than 107 μg/cm^2 were worse in terms of the χ^2 than their thinner counterparts. The similarities between the raw spectra, reflected in the fits, strongly support the conclusion that the relative abundances of the individual Stark states within the $n=3$ level does not change substantially with foil thickness in the thickness region tested. The fits using the symmetry hypothesis gave results consistent with those of the unconstrained fits. The minimum values of reduced χ^2 averaged 0.962, indicating good fits. The fits differ markedly from the statistical weighting, where each of the n^2 states within a given n level is weighted equally (for each value of $m\neq 0$

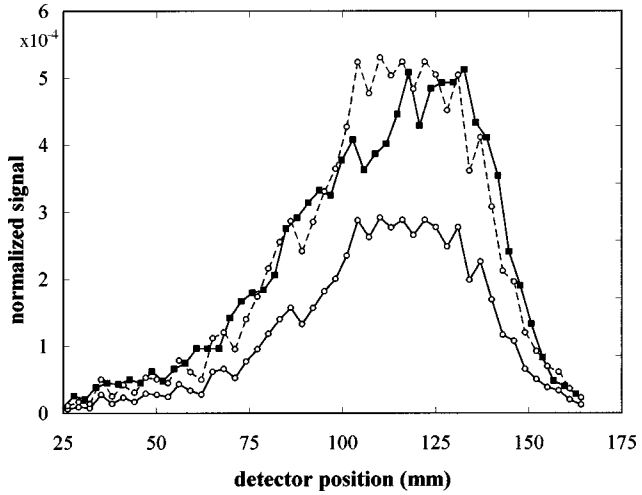

FIG. 9. Spectra in the $n=3$ region from an Al_2O_3 foil placed in the FIF foil box (open circles) of thickness 167 ± 8 μg/cm^2 and an Al_2O_3 foil of thickness 167 ± 8 μg/cm^2 placed 0.6 m downstream in the Gypsy foil box (solid squares). The dashed line through open circles is the FIF foil renormalized to match the area under the spectrum of the foil in the Gypsy foil box.

there are two states). The $m=0$ sublevel, while comprising only $\frac{1}{3}$ of the states in the $n=3$ level, accounts for roughly 50% of the total population in the $n=3$ level. (The observed distribution is close to 3:2:1, suggesting that the states with ±1 are counted as 1.)

B. Al_2O_3 foil raw data and analysis

Four different foil thicknesses of Al_2O_3 foil were tested. The spectrum of an Al_2O_3 foil of thickness 540 μg/cm^2 produced a signal too small to analyze accurately. Of the remaining three foils, two were approximately equal in thickness (161 ± 8 and 167 ± 8 μg/cm^2) and the thickness of the third was 80.9 ± 4.1 μg/cm^2. The 167-μg/cm^2 foil was the only foil used in the FIF foil box; the 80.9- and 161-μg/cm^2 foils were used in the Gypsy foil box. The first comparison is between the foils of like thickness. Figure 9 shows the spectra of the 161- and 167-μg/cm^2 foils renormalized to make the integrated areas equal. Other differences in the spectra are due to the substantial difference in drift time before encountering the Gypsy magnet: the 167-μg/cm^2 foil was placed in the FIF foil box 0.6 m upstream of the 161-μg/cm^2 foil in the Gypsy foil box. Despite these differences, the population fractions determined from these two spectra agree within the uncertainties. Figure 10 displays the fits to the spectra of Al_2O_3 foils of thickness 81 and 161 μg/cm^2, both placed in the Gypsy foil box. The areas of the two spectra were set equal to the area of the 161-μg/cm^2 foil. The spectra clearly show the similarity between the two foils.

A direct comparison between a 50-μg/cm^2 carbon foil and an 81-μg/cm^2 Al_2O_3 foil is shown in Fig. 11. Based on the raw spectra and the fits to the data (shown above), it appears that the population fractions of individual states in the $n=3$ level states are similar for carbon and Al_2O_3 foils.

VI. RESULTS OF ANALYSIS OF $H^0(n=4)$ STATES

A. Carbon foil raw data and analysis

For equal foil thickness, the production of $n=4$ states is lower relative to that of the $n=3$ states [3] by a factor of about 0.40 ± 0.01. The raw data of $n=4$ states produced in carbon foils of different thickness look similar except for a thickness-dependent normalization factor. As in the case of the $n=3$ states, the similarities in the spectra are apparent.

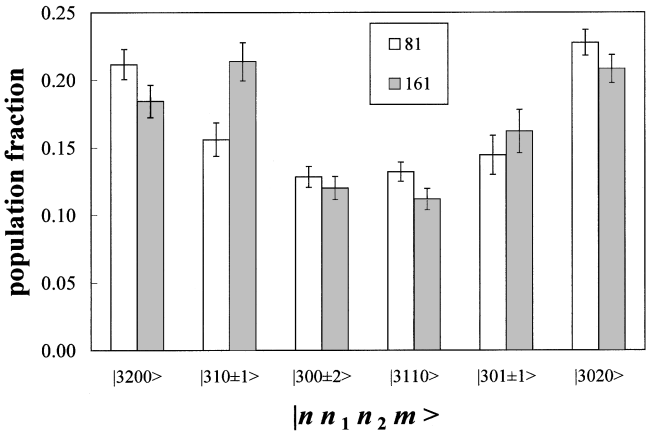

FIG. 10. Population fractions in the $n=3$ level produced by two Al_2O_3 foils of thickness 81 and 161 μg/cm^2 placed in the Gypsy foil box without using the symmetry hypothesis.

The fitting procedure for Stark states in the $n=4$ level is similar to that of the $n=3$ states. The fits are not as good in terms of reduced χ^2 as the fits from the $n=3$ states for three reasons. First, there are ten nondegenerate states in the $n=4$ level, some of whose PDDF curves virtually overlap, as shown in Fig. 6(b). Second, the FWHM of the spectra resulting from stripped $n=4$ states covers only about 30 mm, which is much shorter than the 160 mm FWHM for the $n=3$ spectra. Third, since the overall signal strength is lower than for the $n=3$ states, the $n=4$ states have a lower signal-to-noise ratio. On the other hand, the decay due to spontaneous emission is reduced compared to that of the $n=3$ level. Furthermore, all $n=4$ states strip completely in the 0.6-T field of the Gypsy magnet, unlike in the $n=3$ level, where 30% of state $|3200\rangle$ survives the 1.3-T field.

Fits with and without the symmetry hypothesis were similar. The fit without using the symmetry hypothesis is shown in Fig. 12(a). The populations within the four different m

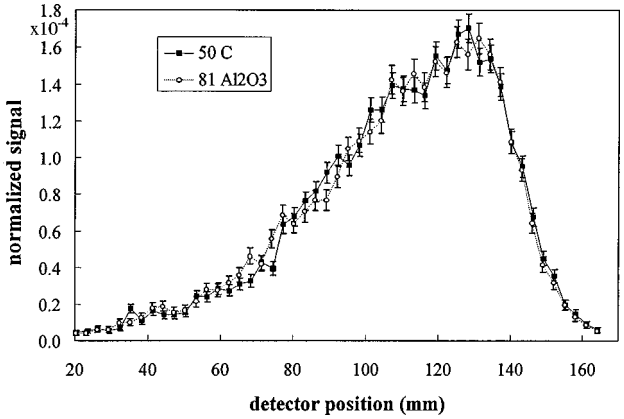

FIG. 11. Comparison of spectra from a 50-μg/cm^2 carbon foil (solid squares) and an 81-μg/cm^2 Al_2O_3 foil (open circles) placed in the Gypsy foil box. A normalization factor was applied to make the areas under the spectra equal.

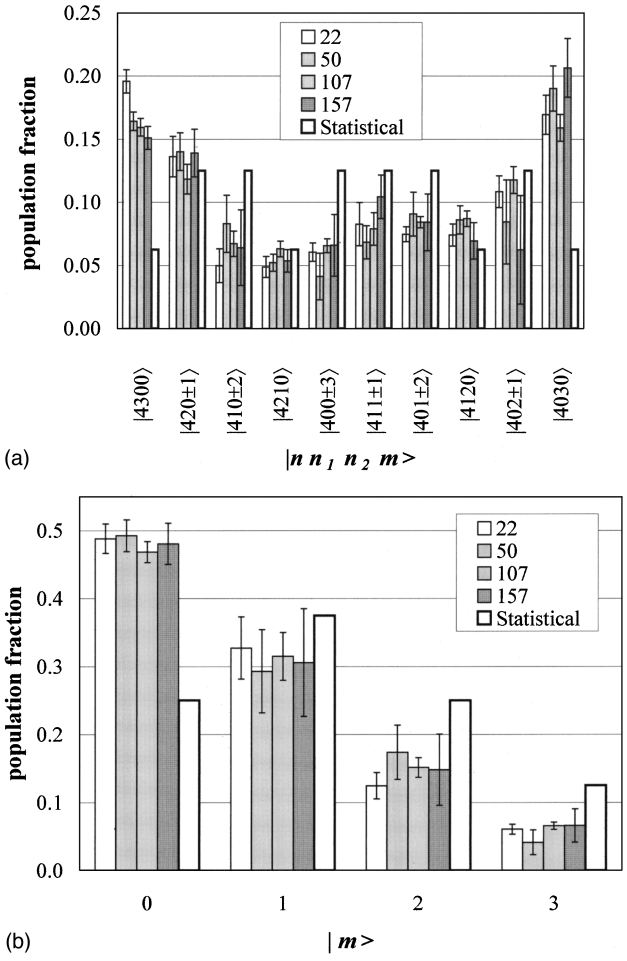

FIG. 12. (a) Population fractions at the foil of $H^0(n=4)$ states for four different carbon foil thicknesses (shown in the legend in units of $\mu g/cm^2$). The values stated are the populations at the foil that include the depletion due to spontaneous decays between the foil and the Gypsy magnet. The fits are not constrained by the symmetry hypothesis in $|k|$. The statistical weights are also shown, where each state with $m \neq 0$ is weighted by $2/n^2$ and states with $m=0$ are weighted by $1/n^2$. (b) Populations in the m sublevel of the $n=4$ level based on the populations in (a). Populations for statistical weighting are also shown. Compared to a statistical distribution, a significantly higher population fraction resides in the $m=0$ sublevel.

sublevels are shown in Fig. 12(b). As with the $n=3$ level, states with $m=0$ comprise a greater fraction of the population distribution than the statistical distribution.

B. Al_2O_3 raw data and analysis

One $n=4$ test of an Al_2O_3 foil placed in the Gypsy foil box was made. A comparison of raw data renormalized to equal areas for this Al_2O_3 foil and a double carbon foil is shown in Fig. 13. The carbon foil spectrum was from a double-foil experiment in which two carbon foils of thickness 107 and 50 $\mu g/cm^2$ were placed in the same foil box about 2 cm apart. The Stark state distribution of the double foil was consistent with that of single carbon foil and consistent with the Al_2O_3 foil.

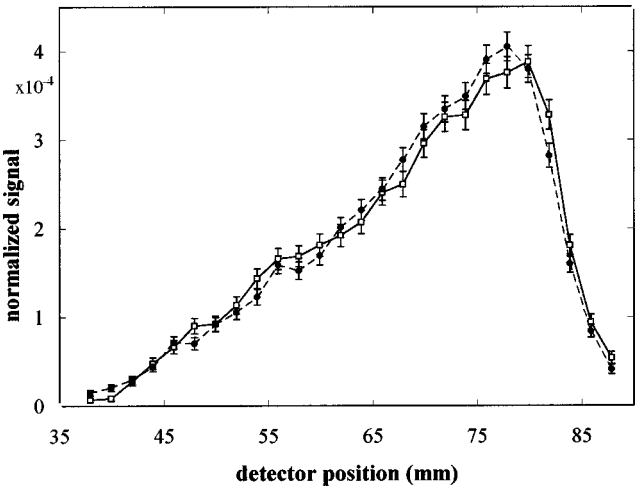

FIG. 13. Comparison of spectra produced with an 81-$\mu g/cm^2$ Al_2O_3 foil (open squares) and a ''double'' carbon foil consisting 50- and 107-$\mu g/cm^2$ foils separated by ~1 cm (solid circles). The spectra were renormalized to make the areas under the curves equal.

VII. FOIL-IN-THE-FIELD EXPERIMENT

A. Introduction

The purpose of the FIF experiments was to determine how applying a motional field in the foil region affects the population distributions of excited states produced in an Al_2O_3 foil. The experimental apparatus was essentially the same as for the studies just described. In these measurements, the 167-$\mu g/cm^2$ Al_2O_3 foil was placed in the 0.16-T field of the FIF magnet. This foil box was 0.6 m upstream of the Gypsy foil box. The data analysis was also essentially the same, but with the increased distance to the Gypsy magnet came an increased fraction of loss due to spontaneous decay. This extra drift distance was accounted for in the calculation of the PDDF curves. Additionally, the drift distance, a low-field region, allows for the evolution of the wave function that mixes states within the same n level. As discussed below, the state mixing causes the $n=4$ FIF field-off spectrum to look considerably different from the spectrum obtained with a similar foil placed in the Gypsy foil box.

B. Results for the $n=3$ level

The experimental data for the FIF on and off cases in the $n=3$ region are shown in Fig. 14. The population distributions at the foil for the field-on and field-off cases are in agreement within the uncertainties. These fits account for the spontaneous decay and for the fact that 30% of the state $|3200\rangle$ that enters the Gypsy field does not field ionize. The fact that the symmetry for the states $|3200\rangle$ and $|3020\rangle$ is present and that the symmetry would not be apparent if the corrections for spontaneous decay and for the partial survival of state $|3200\rangle$ were not included suggests these corrections were quantitatively reasonable. Figure 15(a) shows the population fractions in the $n=3$ level compared with the statistical weighting. Figure 15(b) shows the population fractions within the m sublevels and the statistical weights. As seen in Fig. 8(b), states with $m=0$ are enhanced relative to states with $m \neq 0$. We conclude that the 0.16-T peak FIF field has no appreciable effect on the $n=3$ Stark state distribution.

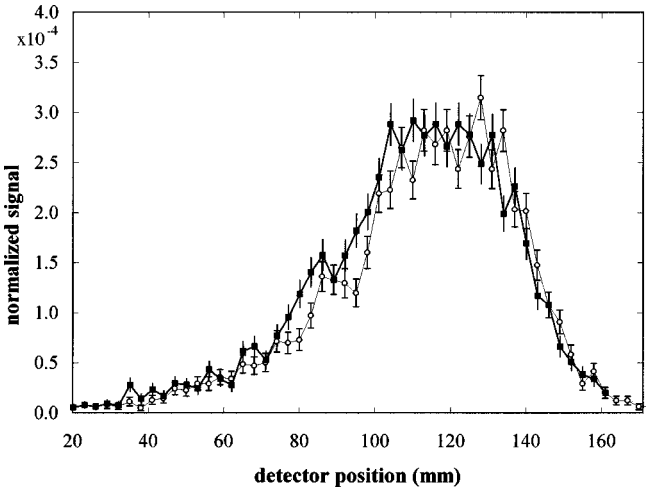

FIG. 14. Comparison between the experimental spectra taken with the FIF magnet on (circles) and off (squares) in the $n=3$ region. The Gypsy magnet was set to a peak field of 1.3 T. The error bars indicate the standard deviations for each data point.

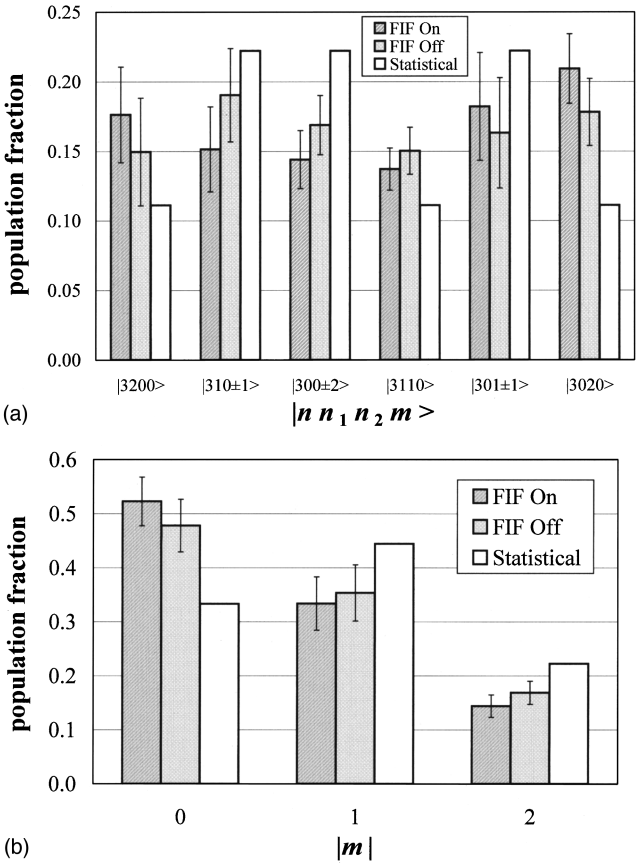

FIG. 15. (a) Population fractions at the foil of $H^0(n=3)$ states comparing the FIF field-off and field-on cases. The fits are not constrained by the symmetry hypothesis in $|k|$. The statistical weights are also shown, where each state with $m\neq 0$ is weighted by $2/n^2$ and states with $m=0$ are weighted by $1/n^2$. (b) Populations in the m sublevel of the $n=3$ level based on the populations in (a). Populations for statistical weighting are also shown. A significantly higher population fraction resides in the $m=0$ sublevel compared to a statistical distribution.

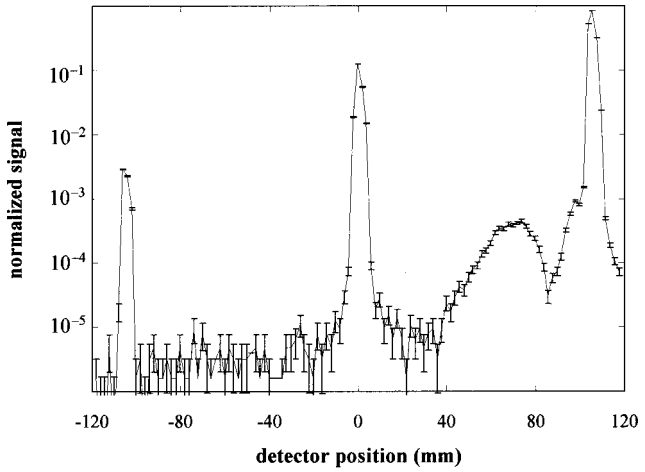

FIG. 16. Normalized signal $(H1\cdot S1\cdot S2)/(S1\cdot S2)$ vs x obtained with the Gypsy magnet set to a peak field of 0.6 T to separate the $n=4$ level from those of higher n. The FIF magnet was turned off. The error bars indicate the standard deviations for each data point. The shoulder beginning near 90 mm is due to ionization of H^0 states in levels $n>4$.

C. Results for the $n=4$ level

The experimental spectrum for the $n=4$ field-off case is shown in Fig. 16. There are marked differences in the Stark state populations for the field-off and field-on spectra shown in Fig. 17. The most striking differences in the two experimental spectra is revealed in the relative abundance of the parabolic state $|4300\rangle$ when the field is on compared to the field-off case. The fit coefficients corresponding to the spectra of Fig. 17 were adjusted for the spontaneous decays to yield the populations produced at the foil, shown in Fig. 18. When the field is imposed on the foil, the population fractions within three m sublevels are the same as for the field-off case within statistical uncertainty, although the state $|4300\rangle$ doubles in population when the field is applied to the foil. The trend of decreasing population for increasing m persists as in the $n=3$ case.

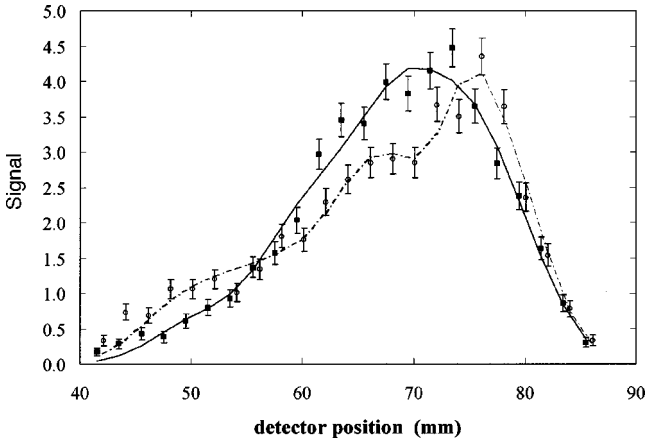

FIG. 17. Fits to the experimental data in the $n=4$ region comparing the 0.16-T field-on (open circles) and field-off (solid squares) cases. The dashed line is the fit when the FIF magnet was set to 0.16 T and the solid line is the fit to the data when the magnet was turned off.

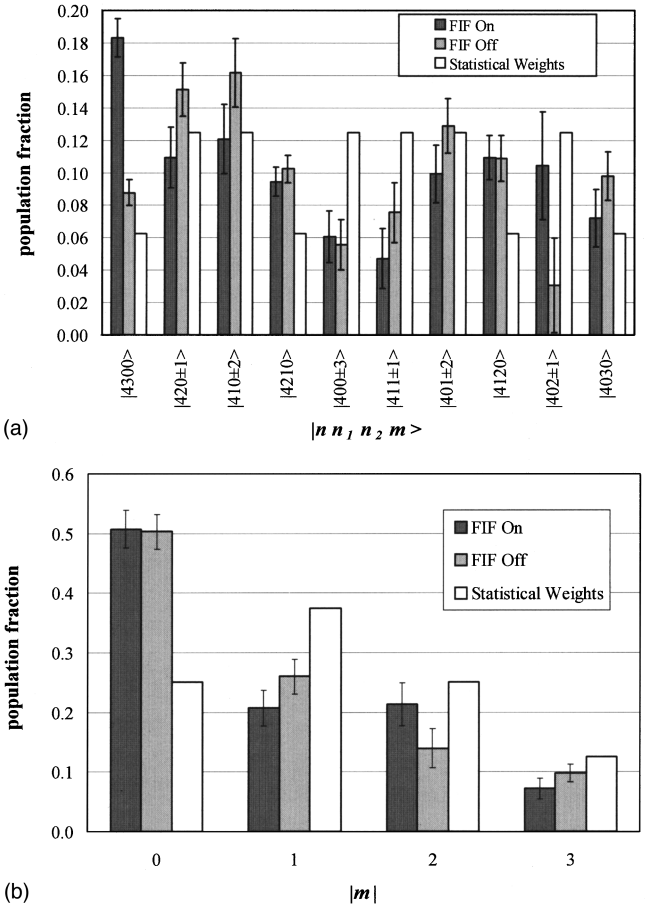

FIG. 18. (a) Population fractions at the foil of $H^0(n=4)$ states comparing the FIF field-off and field-on cases. The fits are not constrained by the symmetry hypothesis in $|k|$. The statistical weights are also shown, where each state with $m\neq 0$ is weighted by $1/n^2$ and states with $m=0$ are weighted by $2/n^2$. (b) Populations in the m sublevel of the $n=4$ level based on the populations in (a). Populations for statistical weighting are also shown. A significantly higher population fraction resides in the $m=0$ sublevel compared with a statistical distribution for both field-on and field-off cases.

D. Comments on the $n=5$ level

The spectra in the $n=5$ region with the field on and field off are shown in Fig. 19. As in the $n=4$ case, there are distinct differences in the spectra depending on whether or not the field was imposed on the foil. The experimental apparatus was unable to resolve individual Stark states of the $n=5$ level. However, since the PDDF for the state most resistant to field ionization, $|5400\rangle$, is peaked near 25 mm and is relatively well separated from it neighbors, it is clear that state $|5400\rangle$ is in greater abundance when the field is on than when the field is off, similar to the $n=4$ case.

E. Comparison of FIF and Gypsy foil box data

As shown in Figs. 15(a) and 10, the population fractions for the Gypsy foil box Al_2O_3 foil tests and FIF field-off case agree within error bars for $n=3$ states. However, it appears that the $n=4$ FIF field-off case is in disagreement with the corresponding test when a similar foil was placed in the Gypsy foil box. Figure 20 shows the apparent discrepancy. When the spectrum of an 81-μg/cm^2 Al_2O_3 foil placed in the

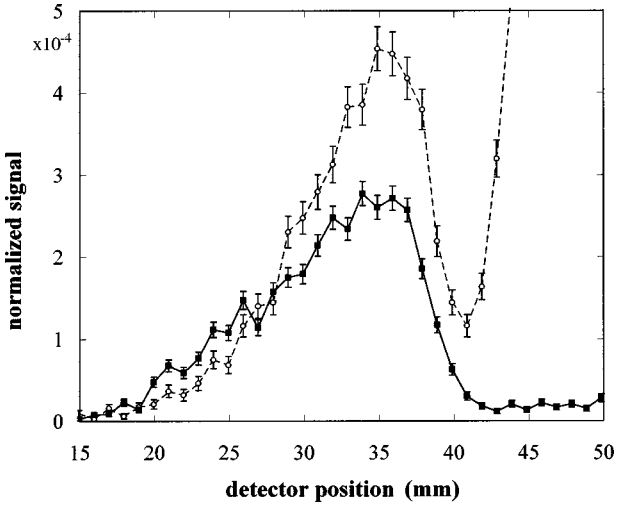

FIG. 19. Normalized signal $(H1\cdot S1\cdot S2)/(S1\cdot S2)$ vs x plotted in the region of the stripped states of the $n=5$ level for the field-on (solid squares) and field-off (open circles) cases. The error bars indicate the standard deviations for each data point. The lines connecting the data points (solid for the field-on case and dashed for field-off case) are to aid in viewing and are not fits to the data. The Gypsy magnet was set to a peak field of 0.27 T for both plots to separate the $n=5$ level from those of higher n. The FIF magnet was set to a peak field of 0.16 T. The shoulder beginning near 45 mm is due to ionization of H^0 states in levels $n>5$.

Gypsy foil box, which looks almost identical to the spectrum of a 161-μg/cm^2 Al_2O_3 foil, is corrected for spontaneous decay to determine the spectrum that would result if the foil were placed at the FIF foil box, the FIF field-off case does not agree with the ''corrected'' spectrum. The corrected spectrum does resemble the field-on case however. Numerous cross-checks were made to ensure the data runs were not interchanged. The fact that the $n=4$ spectra for the FIF field-

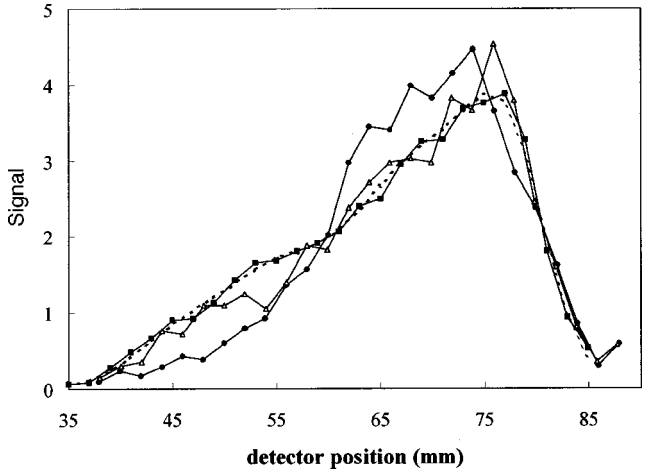

FIG. 20. Comparison between spectra of Al_2O_3 foils at the FIF foil box and at the Gypsy foil box. The solid squares mark the spectrum obtained when the 81-μg/cm^2 foil was placed in the Gypsy foil box. The dashed curve corrects for spontaneous decays between the FIF and Gypsy foil boxes and shows what the spectra would look like if the wave function were not evolving between the FIF foil box and the Gypsy foil box. The open triangle (solid circles) markers show the spectrum obtained when the 161-μg/cm^2 foil is placed in the FIF foil box and the FIF magnet is on (off).

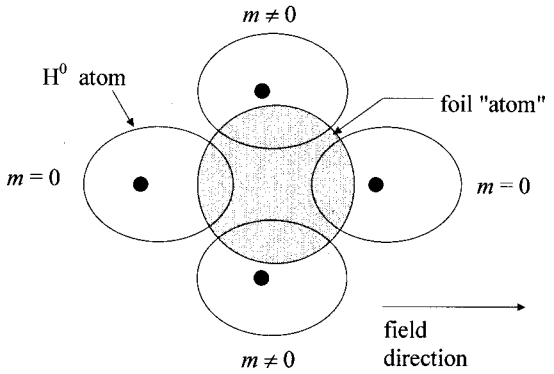

FIG. 21. Qualitative model to explain why the $m=0$ states have a greater chance of being produced with $m=0$ in the interaction of an incoming H^0 atom with a single foil ''atom.'' The beam direction is perpendicular to the page, which is parallel to the foil. A H^0 atom in an excited state collides with the foil atom. If the incoming H^0 atom is to the right or to the left of the foil atom (as shown in the diagram), a state with a zero component of the orbital angular momentum ($m=0$ state) will result. If the H^0 atom impinges from the top or bottom, states with opposite values of $|m| \neq 0$ will result.

off case and the data taken at the Gypsy foil box are quite different is also reflected in the fits. The fit coefficients for some states shown in Figs. 12(a) and 18(a) are in clear disagreement, though the $|m|$ distributions are similar. The cause of apparent discrepancy is discussed below.

VIII. QUALITATIVE DISCUSSION AND CONCLUSIONS

A. Population fractions produced in beam-foil interactions

Two noteworthy features of the experimental results are that (i) the Stark state distribution departed significantly from statistical weighting for the $n=3$ and 4 levels with the relative abundances of $m \neq 0$ being reduced relative to the $m=0$ states and (ii) for the $n=3$ case, the application of the magnetic field on the foil had little effect, but had a pronounced effect for the $n=4$ and 5 levels.

Qualitatively the origin of the apparent enhancement of $m=0$ states can be understood by considering a H^- ion impinging on a spherical scattering center, as shown in Fig. 21. The orbital angular momenta of both electrons is, to a first approximation, zero. Upon passing near a scattering center (i.e., carbon atom) the ion is relieved of one of its electrons, in an interaction that may be regarded as peripheral since we wish to consider that the residual hydrogen atom emerges intact, although possibly excited. Classically we would expect that the residual atom should receive an impulsive torque, perpendicular to both the beam direction and the line joining the atom to the scattering center, causing an increase in orbital angular momentum in the same direction. This same mechanism might also be expected to arise when a hydrogen atom from an earlier interaction is subsequently excited by a peripheral collision. Because the axis of quantization is perpendicular to the beam direction, states with $m=0$ would be expected to be more abundant. Thus the $m=0$ enhancement may have nothing more than a geometrical origin. There are simply more ways to make $m=0$ states.

The invariance of the shape of the raw data indicates that the Stark state fractions produced in the interaction of the 800-MeV H^- beam with thin foils changes appreciably neither with foil thickness nor with the foil materials used in this measurement. Gulley *et al.* [3] discussed the total yield within a given n level versus foil thickness. Here we see no strong dependence of the Stark state fractions on foil thickness. This conclusion holds for both the $n=3$ and 4 levels. Moreover, a gap in the foil interaction makes no large difference; the double-foil $n=4$ spectrum looked nearly identical in shape to the single-foil carbon spectra.

B. Discussion of the foil-in-the-field results

The effects of the external electric field on the population fractions of individual Stark states in the $n=3$ and 4 levels were investigated. The apparent discrepancy between the field-off spectra for the $n=4$, evident in the experimental spectra, is much less evident in the $n=3$ cases. Since the major difference between the two experiments is the placement of the foil, we suspect that the discrepancy depends on the time of flight between the foil and the Gypsy magnet and on principal quantum number n.

The wave function evolves during the flight time between the foil and the Gypsy magnet. The Stark eigenstates (in parabolic coordinates) are, absent fine-structure interactions, degenerate in the zero-field region between the foil and the Gypsy magnet and therefore there is no coupling between them. However, when the parabolic states are projected onto field-free spherical states with the electron spin included, the degeneracy is broken for states of different j. These fine-structure states, as they drift through the field-free region from the production foil to the analyzing Gypsy magnet, develop relative phase differences and decay with different lifetimes, so that the distribution of parabolic states into which they are again projected, to be sorted out by the motional electric field, is altered. The distribution of parabolic states thus depends on the distance of drift from production to analysis. Since the distribution also depends on the relative phases of the states at the production point, which we do not determine, we cannot correct for the changes observed arising from the substantial drift for the FIF measurements. Understanding of the expected differences between the distributions of the $n=3$ and 4 levels would require detailed modeling beyond the scope of the present paper. It should be emphasized, however, that differences in the distributions for $n=4$ states produced with the field on and field off are significant and indicate the presence of stripping propensities, dependent on the strength of the applied motional electric field, which have not yet been explained theoretically.

ACKNOWLEDGMENTS

The authors wish to thank J. Hontas, J. DeMoss, and C. Allen of the University of New Mexico for their assistance in designing and building the scintillator translation stage; the technical staff of LAMPF, especially L. Quintana, for their preparation and maintenance of the beam line and operation of the beam; D. Viera, J. Tesmer, and M. Borden for assistance with the foil density measurements; and F. Roybal for assistance with the installation of the foils into the beam line. We also thank C. Planner of the Rutherford Appleton Labo-

ratory for providing the Al_2O_3 foils used in the experiment. P.B.K. is grateful to T. Bergemann for providing the results of his calculations and to A. Underhill for providing a key reference. This work was supported by the U.S. Department of Energy, Division of Chemical Sciences, Office of Basic Energy Sciences, Office of Energy Research.

[1] Joachim Burgdörfer and John Gibbons, Phys. Rev. A **42**, 1206 (1990).
[2] Benoit Gervais *et al.*, Phys. Rev. A **53**, 3201 (1996).
[3] M. S. Gulley *et al.*, Phys. Rev. A **53**, 3201 (1996).
[4] P. Kürpick, C. O. Reinhold, J. Burgdörfer, and B. Gervais, Phys. Rev. A **58**, 2183 (1998).
[5] Richard Hutson, Los Alamos National Laboratory Report No. PSR-92-015, 1992 (unpublished).
[6] R. J. Macek, in *Machine Studies at the Los Alamos Proton Storage Ring*, Proceedings of the International Collaboration on Advanced Neutron Sources, 1993 (Science and Engineering Research Council, Chilton, UK, 1993), Vol. II, pp. A25–A32.
[7] W. S. Bickel and A. S. Goodman, Phys. Rev. A **48**, 1 (1996).
[8] H.-D. Betz, D. Röschenthaler, and J. Rothermel, Phys. Rev. Lett. **50**, 34 (1983).
[9] J. Rothermel, H.-D. Betz, and F. Bell, Nucl. Instrum. Methods Phys. Res. **194**, 341 (1982).
[10] Jürgen Kemmler, Joachim Burgdörfer, and Carlos O. Reinhold, Phys. Rev. A **44**, 2993 (1991).
[11] Y. Yamazaki *et al.*, Phys. Rev. Lett. **61**, 2913 (1988).
[12] A. H. Mohagheghi, Los Alamos National Laboratory Report No. LA-11925-T, 1990 (unpublished).
[13] A. H. Mohagheghi *et al.*, Phys. Rev. A **43**, 1345 (1991).
[14] H. C. Bryant (unpublished); P. B. Keating (unpublished); P. B. Keating, Ph.D. dissertation, University of New Mexico, 1996 (unpublished).
[15] H. A. Bethe and E. E. Salpeter, *Quantum Mechanics of One- and Two-Electron Atoms* (Plenum, New York, 1977), p. 231.
[16] R. J. Damburg and V. V. Kolosov, in *Rydberg States of Atoms and Molecules*, edited by R. F. Stebbings (Cambridge University Press, Cambridge, 1986).
[17] Andrew J. Jason, Daniel W. Hudgings, and Olin B. van Dyck, IEEE Trans. Nucl. Sci. **NS-28**, 2704 (1981).
[18] J. D. Jackson, *Classical Electrodynamics*, 2nd ed. (Wiley, New York, 1975).
[19] Charles W. Planner of the Rutherford Appleton Laboratory (United Kingdom) provided the Al_2O_3 foils used in this experiment.
[20] Mark S. Gulley and W. A. Miller, Los Alamos National Laboratory Report No. LAUR-95-210, 1995 (unpublished).
[21] W. H. Press, S. A. Teukolsky, W. T. Vetterling, and B. P. Flannery, *Numerical Recipes in C: The Art of Scientific Computing*, 2nd ed. (Cambridge University Press, Cambridge, 1992).
[22] Thomas Bergeman (private communication).